Improved Cu- and Zn-based catalysts for CO2 hydrogenation to methanol

Djaouida Allam, Simona Bennici, Lionel Limousy, Smain Hocine

Improved Cu,Zn-based catalysts for CO_2 hydrogenation to methanol

Catalyseurs améliorés à base de Cu et Zn pour l'hydrogénation de CO_2 en méthanol

DjaouidaAllam[1], Simona Bennici[2, 3,*], Lionel Limousy[2, 3], and Smain Hocine [1]

[1]*Laboratoire de Chimie Appliquée et de Génie Chimique Université M. Mammeri de Tizi-Ouzou BP .17 R.P 15000 Tizi-Ouzou, Algeria.*

[2]*Université de Haute-alsace, CNRS, IS2M UMR 7361, F-68100 Mulhouse, France*

[3]*Université de Strasbourg, France*

Résumé

Dans cette étude, des catalyseurs binaires et ternaires (CuO-CeO_2, ZnO-CeO_2, CuO-ZnO-CeO_2 et CuO-ZnO-Al_2O_3) ont été utilisés pour l'hydrogénation CO_2 en méthanol à pression atmosphérique. L'influence de la dispersion des métaux, de la formation de spinelles et des propriétés de surface sur les performances catalytiques ont été étudiées.

Les catalyseurs, préparés par la méthode polyol en utilisant du polyéthylène glycol en tant que solvant, présentent des propriétés améliorées en termes de dispersion des oxydes métalliques, de morphologie (forme de type éponge pour les catalyseurs contenant CeO_2) et de variétés d'espèces métalliques et d'oxydes métalliques à la surface. De plus, les catalyseurs CuO-ZnO-CeO_2 et Cu-ZnO-Al_2O_3 présentent une activité et une sélectivité supérieures à celles de catalyseurs préparés par des procédés plus conventionnels, pour la synthèse du méthanol par hydrogénation de CO_2.

Abstract

In this work the influence of the metal dispersion, the spinel formation, and the surface properties of binary and ternary catalysts ($CuO-CeO_2$, $ZnO-CeO_2$, $CuO-ZnO-CeO_2$ and $CuO-ZnO-Al_2O_3$) was evaluated. The catalysts, prepared by polyol method using polyethylene glycol as a solvent, have been tested in the CO_2 hydrogenation to methanol performed at atmospheric pressure.

The catalysts prepared by polyol method presented improved properties in terms of metal oxide dispersion, morphology (i.e. sponge like shape for the CeO_2-containing catalysts), and a large variety of metal and metal oxide species on the surface. Moreover, the $CuO-ZnO-CeO_2$ and $CuO-ZnO-Al_2O_3$ catalysts exhibited a higher activity and selectivity in the methanol synthesis by CO_2 hydrogenation than those displayed by catalysts prepared by more conventional methods.

Keywords: *CO_2 valorization; polyol synthesis; methanol synthesis; oxide catalysts*

1. Introduction

The concentration of carbon dioxide (a greenhouse gas) inexorably increases in the atmosphere. Various methods are currently examined to decrease the CO_2 concentration or to convert it into valuable chemical products. The utilization of CO_2 as a feedstock for the synthesis of high added value chemicals is a promising alternative for CO_2 abatement [1,2]. The simplest way to utilize carbon dioxide is the hydrogenation into valuable compounds, such as methanol (MeOH) and DME (dimethyl ether) [3-8]. Such conversion is often performed on copper-based catalysts. Industrial methanol synthesis is performed by catalytic hydrogenation of syngas ($H_2/CO/CO_2$) over $Cu/ZnO/Al_2O_3$-type catalyst. Unfortunately, the industrial $Cu/ZnO/Al_2O_3$ catalyst are not active nor selective in CO_2 hydrogenation. Previous

published research works demonstrated that the use of industrial catalysts brings to very low hydrogenation conversions of CO_2 to methanol [9].

This issue can be overcome by developing suitable catalysts, which can effectively convert carbon dioxide to methanol [10-13]. Even if copper based materials are promising catalysts for the hydrogenation of CO_2 [14-19], further investigations are required for developing new catalytic materials able to give high conversion of CO_2 and improved selectivity to MeOH.

In order to improve the catalytic performance for methanol synthesis from H_2/CO_2 feeding gas, CuO/ZnO catalysts have been widely modified by adding various activators or other metals (Zr, Si, La, Ti, Cr, Ga, Ce, Fe, Nb, Pd...) [20-25]. The effect of the support was also extensively studied. The type of support affects both CO_2 conversion and methanol selectivity, and, in general, basic oxides such as La_2O_3, Sm_2O_3, Nb_2O_5, In_2O_3 and ThO_2 [26-27], used as supports, favor the methanol formation. The preparation methods have also a considerable influence on the catalytic performance [28-30]. Several methods such as co-precipitation [31-35], impregnation [36-38], and sol–gel [38-39] have been developed to prepare copper-based oxide catalysts. Moreover, the co-precipitation synthesis was improved by addition of reducing agents, such as chitosane [14], and $NaBH_4$ [15]. Surfactant-assisted co-precipitation [16], solvent-free routine combustion [40], and micro-fluidic co-precipitation [41] are novel synthesis methods that allow obtaining a good repeatability of the synthesis, and an improved homogeneity of the phases present in the catalyst. Other methods, such as impregnation and sol–gel, can also produce catalysts with large specific surface areas and high CuO dispersion [42]. Polyol synthesis represents a good alternative to the classical synthesis methods. In particular, it presents many advantages, such as the possibility to precisely modulate the stoichiometric ratio, the homogeneous mixing of the various components, the low cost and the short reaction time. Therefore, polyol synthesis reveals to be an attractive technique for the synthesis of nano-oxide powders.

$CuO/ZnO/Al_2O_3$-type catalysts obtained by polyol synthesis have been successfully applied in the Reverse Water Gas Shift Reaction RWGS [43], in the alcohol-assisted low temperature methanol synthesis from syngas [44], and in methanol reforming [45].

The polyol method [46-47] permits to synthesize nano-sized metallic powders with uniform size distribution and shape [46-48]. In recent years, the polyol method has been studied by many researchers [49-52]. These investigations showed that the crystallites' size and shape [46] can be controlled by varying the reduction temperature, the pH, and the nucleation-protective agent concentration [49-53]. Up to now, and at our knowledge, no attempts to prepare Cu/ZnO catalyst for methanol production using the polyol method have been done. In a typical polyol synthesis, polyols (ethylene glycol, diethylene, glycerol, and tetraethylene glycol) act at the main time as the reaction medium and as the reducing agent. The metal precursor is reduced through a redox reaction between the metal precursors and the polyolic species. Therefore, the reaction temperature is an important parameter, because the oxidation potential of polyol chemicals decreases with the increasing of the reaction temperature **[**49, 54-55]. Nucleation-protective chemicals such as polyvinylpyrrolidone (PVP) are occasionally employed to prevent sintering and agglomeration of metal particles [54-55]. The various published researches indicate that the choice of the preparation conditions strongly affects the activity of catalysts prepared by polyol method.

In the present work, the so-called "polyol method" has been used to obtain improved catalytic materials for the hydrogenation reaction of CO_2 to methanol. The influence of the metal dispersion, spinel formation and surface properties of binary and ternary catalysts ($CuO-CeO_2$, $-ZnO-CeO_2$, $CuO-ZnO-CeO_2$ and $CuO-ZnO-Al_2O_3$), prepared by polyol method using polyethylene glycol as solvent, is evaluated in the CO_2 hydrogenation to methanol at atmospheric pressure, used as test reaction.

2. Experimental

2.1. Preparation of binary and ternary polyol catalysts

Two binary catalysts (labeled ZnO-CeO_2, and CuO-CeO_2, with molar ratio of Zn/Ce and Cu/Ce equal to 1) and two ternary catalysts (labeled CuO-ZnO-CeO_2, and CuO-ZnO-Al_2O_3, with Cu/Zn/Ce and Cu/Zn/Al molar ratios of 1/1/2) were prepared by polyol method. The reaction temperature and the choice of the solvent were selected referring to the available investigations reported in the literature [44, 45]. These experimental conditions seem to favor the formation of nanocrystallites. Differently from the synthesis reported in these already published works, nitrate-base precursors were used in the present research instead of Me-acetates. In fact, nitrates do not participate to secondary reactions like those operated by acetates that can react to form methyl acetate and ethyl acetate. Firstly, copper nitrate $Cu(NO_3)_2.2.5H_2O$ (Sigma-Aldrich 98%), and/or zinc nitrate $Zn(NO_3)_2.6H_2O$ (Sigma-Aldrich 99%) were dissolved in polyethylene glycol $(C_2H_6O_2)_n$ (Sigma-Aldrich 99%, d=1.13g/ml). The solution at pH=2 was then heated up, step by step, and kept under stirring for 1 hour at 70°C, 2h at 120°C, and 2h at 180°C. Cerium and/or aluminum nitrates $Ce(NO_3)_3.6H_2O$ and/or $Al(NO_3)_2.1H_2O$ from (Sigma-Aldrich 99%) were then added to the initial solution under vigorously stirring for 4 hours at the same temperature (180°C). The formation of a precipitate was observed. The suspension was cooled down at 100°C, and NH_4OH was added dropwise to reach a pH of 7. The resulting suspensions were kept under vigorous stirring at 100°C for 24 h. Finally, the formed gel was dried at 180°C for 72 h, and then calcined in air at 450°C for 5h.

2.2. Characterization techniques

Thermogravemetric analyses (TGA) were performed with a TGA/DSC 1 LF 1100 STARS system from METTER TOLEDO. The samples were heated-up at 5°C/min under air flow (100 mL/min) from room temperature to 500°C.

The XRD patterns were acquired with a PANalytical MPD X'Pert Pro diffractometer operating with Cu Kα radiation, λ = 0.15406 nm at 40 mA and 45 kV with a scan rate of 2° min^{-1}. The data were collected in the 5-60° 2θ range. The diffraction patterns were analyzed using the Joint Committee on Powder Diffraction Standard (JCPDS). CuO, ZnO, and CeO_2 crystallite size were calculated by means of the Scherrer equation:

$$d = \frac{0.89\,\lambda}{\beta \cos\theta} * \frac{180}{\pi} \qquad (1)$$

where d is the diameter of the crystallite, λ the X-ray wave length, and β is the width at half height (FWHM) of the peak.

N_2-adsorption isotherms of the samples were acquired at -196°C in a Micromeritics ASAP2420 apparatus. 0.25 g of catalyst was pretreated at 300°C during 10 h under vacuum (~50 m Torr). The specific surface area was calculated applying the multi-Pont BET method [56], while the pore size distribution was obtained by applying the BJH method [57] to the desorption branch of the isotherm.

Scanning electron microscopy coupled to energy dispersive X-ray spectroscopy (SEM-EDX) was performed on a PHILIPS XL 30 instrument (electrons acceleration voltage of 15 kV).

X-ray photoelectron spectroscopy (XPS) measurements were performed on a Kratos Axis Ultra DLD spectrometer equipped with a monochromatic micro focused Al Kα (1486.6 eV and Mg Kα=1253.6 eV) X-ray exciting source. The pass energy of the analyzer was set at 40 eV. The adventitious C1s peak (284.6 eV) was used as internal reference with an accuracy of ±0.3 eV. XPS was used to evaluate the oxidation state of copper, zinc and cerium species. O 1s, Cu 2p, Zn 2p, Ce 3d and Al 2p species were quantified by analysis of the survey XPS

spectra. The binding energy of C 1s, O 1s, Cu 2p, Zn 2p Ce 3d, and Al 2p were analyzed in order to identify the associated surface species and the relative atomic concentration.

2.3 Catalytic tests

The catalytic hydrogenation of carbon dioxide to methanol was evaluated in a fixed-bed continuous flow reactor. During each test, 0.3 g of catalyst was pretreated with hydrogen at 300°C for 3 hours. After the reduction step, the catalyst was exposed to a H_2/CO_2 (1/9 volume ratio) flow at different reaction temperatures (190-240°C). The feeding mixture and the reaction products were analyzed online with a gas chromatograph (Shimadzu GC-2014) equipped with FID and TCD detectors. CO_2 conversion (X) and products' selectivity were calculated as follows, using the quantitative correction factor kf, and peaks area (S) for the different species:

$$\mathrm{X\,CO_2(\%)} = \frac{S_{CO_2\,in} - S_{CO_2\,out}}{S_{CO_2\,in}} \times 100 \times kf_{CO_2} \qquad (2)$$

$$\mathrm{CH_3OH\ selectivity\ (\%)} = \frac{S_{CH_3OH\,out}}{\mathrm{X\,CO_2}} \times 100 \times kf_{CH_3OH} \qquad (3)$$

$$\mathrm{CH_4\ selectivity\ (\%)} = \frac{S_{CH4\,out}}{\mathrm{X\,CO_2}} \times 100 \times kf_{CH_4} \qquad (4)$$

3. Results and discussions

3.1. Characterization of catalysts

3.1.1. Thermal behavior

The catalysts thermal behavior, before and after calcinations, is shown in Fig.1. The samples mass continuously decreased with the temperature. For the catalysts before calcination, the TGA curves showed three main events connected to the residual precursors decomposition (Fig.1a**)** (indeed, the most part of the precursors has been eliminated by the thermal treatment during the synthesis).

A first mass variation in the 0.5- 2.5% range was observed up to 250 °C, and was attributed to the loss of water (physi- and chemi-sorbed) as well as to the decomposition of residual nitrates from the precursors. The second and highest mass loss (0.5-3%), between 250 and 350°C, was probably related to the elimination of polyethylene glycol. The third step, at temperature higher than 350°C, corresponded to the lowest mass loss (0.5%), and was attributed to the decomposition of hydroxyl groups, leading to metal oxide formation. After calcinations (Fig. 1b), the catalyst showed a low mass loss (below 2%), attributed to the release of physisorbed water (under 150 °C), and the decomposition of carbonates formed by reaction with atmospheric CO_2. The presence of carbonates was observed also by XPS (as described in section 3.1.3).

3.1.2. Structure and morphology of the catalysts

The X-ray diffractograms of the calcined bimetallic and trimetallic catalysts are displayed in Fig.2. For the three calcined catalysts, CuO-CeO_2, ZnO-CeO_2, and CuO-ZnO-CeO_2, only the diffraction peaks relative to the CuO, ZnO, and CeO_2 phases could be clearly identified. The diffraction peaks centered at 28.6, 33.1, 47.5, 56.3, 59.1 and 69.0° 2θ, corresponding respectively to the (111), (200), (220), (311), (222) and (400) diffraction planes of cubic CeO_2 [58-59], were observed for the ZnO-CeO_2, CuO-CeO_2, and CuO-ZnO-CeO_2 catalysts. For the ZnO-CeO_2 and CuO-ZnO-CeO_2 samples, diffractions at 31.7, 34.5, 36.2, 62.9 and 69.0° 2θ indicated the presence of hexagonal ZnO [31,58,60-61] and corresponded respectively to the (100), (002), (101), (103) and (201) planes. The cubic CuO phase [31,58,60], present in the CuO-CeO_2 and CuO-ZnO-CeO_2 samples, was characterized by broad diffraction lines at 35.5 and 38.7° 2θ corresponding to the (-111) and (111) planes. Broad diffraction lines at 2θ = 35.5 38.7, 61.5 and 68.1° indicated the presence of CuO and corresponds respectively to the (-111), (111), (-202), (-113) and (-220) planes. In addition to CuO, $CuAl_2O_4$ and $ZnAl_2O_4$ spinel could be identified in the CuO-ZnO-Al_2O_3 sample. The

diffraction peak of $CuAl_2O_4$ and $ZnAl_2O_4$ were superposed and placed at 31.2, 36.8, 55.6, 59.3, and 65.2° 2θ. No diffraction peaks relative to ZnO could be identified in CuO-ZnO-Al_2O_3; all zinc was present as spinel, $CuZnAl_2O_4$.

The metal oxide crystallite dimensions were evaluated applying the Scherrer equation to the main diffraction peak of each phase, and the results are reported in Table 1. ZnO crystallites size of 20-30 nm was calculated in the binary ZnO-CeO_2 catalyst. CuO crystallites, in the 10-20 nm dimension range, were detected for the CuO-CeO_2 catalyst (Table 2). The CuO (6 nm) and ZnO (12 nm) crystallites were much smaller for the ternary CuO-ZnO-CeO_2 sample, indicating that the presence of zinc and copper oxides together ameliorate the oxides distribution and dispersion during the synthesis procedure.

The nitrogen adsorption-desorption isotherms of the various polyol samples (acquired at -196 °C) are shown in Fig.3a. The catalysts isotherm shows a continuous increase of adsorbed nitrogen over the whole P/P0 range, with a relatively steep increase at P/P0 ≥ 0.85. For the all catalysts, the N_2 adsorption isotherms (Fig.3b) were of type (II) [62] with no plateau at high *P*/*P*0 values, which is usually observed for materials with macropores or inter-particular mesoporosity [63]. H4-type hysteresis was observed for the CuO-ZnO-Al_2O_3 sample, and H3-type for the ZnO-CeO_2, CuO-CeO_2, and CuO-ZnO-CeO_2 samples [64]. These types of hysteresis are typical of lamellar compounds or slit-shaped pores [65].

All materials presented relatively low porous volumes (Table 1, 3th column), as expected for this kind of preparation that produces bulk oxides. Fig. 3b represents the pore size distribution of the catalysts. All catalysts presented a certain mesoporosity centered in the 17-23 nm range. The presence of macropores (up to 150 nm) was observed for the three samples containing CeO_2, while even larger pores were present in the CuO-ZnO-Al_2O_3 sample.

The presence of copper oxide seems to improve the specific surface area of the catalysts (in the 30-38 $m^2.g^{-1}$ range), as reported in Table 1. The catalyst with the lower surface area (18

$m^2.g^{-1}$) was $ZnO\text{-}CeO_2$. This behavior is probably connected to the improved pore volume that can be obtained in the presence of the copper precursor, that end up into a higher internal surface area. Indeed, $ZnO\text{-}CeO_2$ presented the lowest pore volume, and the hysteresis between the adsorption and desorption isotherms was almost absent.

Table 1: morphological and structural properties of the catalysts

Sample	S_{BET} ($m^2.g^{-1}$)	V_{pore}[b] ($cm^3.g^{-1}$)	D_{pore} (nm)	Crystallite size with XRD analysis (nm)[b]			
				CuO	ZnO	CeO_2	$Cu,ZnAl_2O_4$
$CuO\text{-}CeO_2$	32	0.07	17	10-20	-	5	-
$ZnO\text{-}CeO_2$	18	0.03	20	-	20-30	5	-
$CuO\text{-}ZnO\text{-}CeO_2$	38	0.12	22	6	12	5	NA
$CuO\text{-}ZnO\text{-}Al_2O_3$	30	0.04	23	20-30	-	-	30-40

[a] *Determined from desorption branch of N_2 adsorption isotherm by BJH model*
[b] *Crystallite size calculated by Scherrer equation*

The morphology of the different calcined $CuO\text{-}CeO_2$, $ZnO\text{-}CeO_2$, $CuO\text{-}ZnO\text{-}CeO_2$, $CuO\text{-}ZnO\text{-}Al_2O_3$ samples was investigated by scanning electron microscopy, and the acquired images are presented in Fig.4. The catalysts containing CeO_2 showed a sponge-like morphology, as reported in Fig.4 for the $CuO\text{-}CeO_2$ (a-c), $ZnO\text{-}CeO_2$ (d-f), and $CuO\text{-}ZnO\text{-}CeO_2$ (g-i) samples. The three ceria-containing samples were characterized by the presence of round-shaped cavities and pores of various dimensions, well distributed in the sample catalyst structure. $CuO\text{-}ZnO\text{-}Al_2O_3$ presented a different morphology (Fig.4 j-l), with well-developed and thin plate-shaped bonded sheets in the 1 to 5 μm dimension interval. The presence of macropores was confirmed by these images and linked to the formation of gas bubbles during the preparation step, due to the decomposition of the metal oxide precursors.

EDX analysis showed a very homogeneous distribution of the different oxides in all samples.

3.1.3. Chemical composition and surface properties

Photoelectron spectroscopy was used to evaluate the oxidation state of copper, zinc and cerium species in the CuO-ZnO-CeO_2 and CuO-ZnO-Al_2O_3 calcined catalysts, as well as to evaluate their surface chemical composition (Tables 2). All elements (Cu, Zn, Ce, Al, and O) were present at the samples' surface (Table 2). The survey XPS acquisition permitted to quantify the various atoms (O 1s, Cu 2p, Zn 2p, Ce 3d and Al 2p) for the two trimetallic catalysts. Clear differences in the surface elements were observed for the two samples. Zn concentration was particularly low on the surface of the CuO-ZnO-CeO_2 sample (0.53 %). At the contrary a big amount of carbon was detected on its surface (24.31 %). Because the most part of carbon on the surface of CuO-ZnO-CeO_2 could be assigned to residual contamination or hydrocarbon chains, as described later in this section, these results can suggest that the carbon pollution presented a higher affinity for Zn, thus selectively covered at the extreme surface. Less dramatic differences were identified in the CuO-ZnO-Al_2O_3 sample that showed similar concentrations of copper and zinc on the surface.

No N1s XPS peak (generally placed around 400.3 eV), related to nitrate (NO_3^-) species (salt precursors) has been identified for the CuO-ZnO-Al_2O_3 and CuO-ZnO-CeO_2 catalysts, as an indication of the complete decomposition of nitrated after calcination.

The binding energy of C 1s, O 1s, Cu 2p, Zn 2p Ce 3d, and Al 2p of the two trimetallic catalysts are listed in Table 2, as well as the associated surface species and their atomic concentration.

The Cu 2p spectrum of both CuO-ZnO-CeO_2 and CuO-ZnO-Al_2O_3 (Fig.5) catalysts presented the characteristic spin-orbit split Cu $2p_{1/2}$ and Cu $2p_{3/2}$ peaks, with their shake-up satellites of Cu^{2+} [66]. Binding energies, in the 932.0-932.8 and 933.2-934.6 eV range, are characteristic of Cu^+ and Cu^{2+}, respectively [67-68]. These two contributions could be identified in the CuO-ZnO-CeO_2 sample (upper spectrum in Fig.5). The large and strong peak centered at 932.7 eV was then attributed to Cu^{2+} and/or Cu^+ species, while the small and broad peak

centered at 934.9 eV was assigned to Cu^{2+} species [69]. For the CuO-ZnO-Al_2O_3 sample (Fig.5), the Cu $2p_{3/2}$ peak presented two contributions characteristic of Cu^{2+} species; the first one was observed at 933.61 eV and related to copper oxide, while a second contribution, at a higher binding energy (935.66 eV), was assigned to Cu^{2+} in the $CuAl_2O_4$-like environment (the presence of the spinel structure, $CuAl_2O_4$, was also observed by XRD analysis). Indeed, the shift to higher binding energy is indicative of a charge transfer from Cu^{2+} towards $Al_2O_4^{2-}$ [70-71]. The intensity ratio of the satellite peak to the related main peak (I_{sat}/I_{pp}) was of 0.17, for the CuO-ZnO-CeO_2 catalyst, and of 0.44 for CuO-ZnO-Al_2O_3. The lower I_{sat}/I_{pp} value is characteristic of well dispersed copper oxide species in an octahedral coordination environment, while the higher value is symptomatic of a coordination change, most probably due to the formation of the spinel [72]. In addition, the contribution at around 529 eV of the O 1s spectra can also be assigned to the presence of Cu^{2+} and Cu^{+} (see Table 2).

Table 2: Surface elements' presence as determined by XPS analysis

Orbital	CuO-ZnO-CeO_2			CuO-ZnO-Al_2O_3		
	B.E. (eV)	Species	At (%)	B.E. (eV)	Species	At (%)
C 1s	284.98	C-C	16.54	285.01	C-C	2.46
	286.53	C-OR	0.60	286.56	C-OR	0.28
	287.98	C=O	2.55	288.01	C=O	0.40
	289.48	O=C-O	4.62	289.47	O=C-O	0.89
O 1s	529.49	Cu-O	6.97	529.80	Cu-O	9.02
	529.43	Ce^{4+}/Cu-O	29.07	531.71	Al-O	33.22
	530.90	Ce^{3+}/Zn-O	4.17	530.80	Zn-O	8.51
	531.90	$(CO_3)^{2-}$	7.04	531.40	$(CO_3)^{2-}$	2.64
Cu 2p	932.75	Cu^{2+}/Cu^{+}	5.87	933.61	Cu^{2+}	4.31
	934.91	Cu^{2+}/Cu^{+}	0.97	935.66	Cu^{2+}	1.42
	940.92	Cu^{2+}/Cu^{+}	0.99	940.87	Cu^{2+}	1.68
	943.54	Cu^{2+}/Cu^{+}	0.78	943.43	Cu^{2+}	1.65
Zn 2p	1021.56	ZnO	0.53	1021.87	ZnO	7.71
Ce 3d	881.00 (V^0) 899.39 (U^0)	Ce^{3+}	0.92	-	-	-
	882.44 (V) 900.76 (U)	Ce^{4+}	4.42	-	-	-
	884.95 (V^I) 903.20 (U^I)	Ce^{3+}	3.80	-	-	-
	888.70 (V^{II}) 907.36 (U^{II})	Ce^{4+}	5.33	-	-	-
	898.16 (V^{III})	Ce^{4+}	4.82	-	-	-

	916.34 (U^{III})					
Al 2p	-	-	-	74.47	Al^{3+}	24.86

The Zn $2p_{3/2}$ XPS spectra for the two trimetallic catalysts was characterized by one defined peak around 1021-1022eV that could be assigned to Zn^{2+} species. The presence of ZnO have been also confirmed by the O 1s band centered at 530.8 eV [73-74]. The XPS signal of CuO-ZnO-CeO_2 was much less intense than that of CuO-ZnO-Al_2O_3, indicating the higher ZnO concentration on the CuO-ZnO-Al_2O_3 surface (8.68 $\%_{atom}$ for CuO-ZnO-Al_2O_3 and 0.53 $\%_{atom}$ for CuO-ZnO-CeO_2 catalysts.

The presence of carbon was detected on the surface of both samples. The C 1s spectra is reported in Fig.6, for the CuO-ZnO-CeO_2 and CuO-ZnO-Al_2O_3 catalysts. In both cases the spectra were composed of two contributions; the first, centered at 289.5 eV was assigned to carbonate species, while the more intense band, at around 285 eV, to residual contamination or hydrocarbon chains, probably deriving from the polyethylene glycol used during the catalyst synthesis. Indeed, cerium oxide and reduced cerium are known to react with CO_2 (present in the atmosphere, for example), and give rise to carbonate species on the surface [75]. The carbonate band was much less intense for the CuO-ZnO-Al_2O_3 catalyst, and the corresponding atomic percentage was about 1.3% instead of 7.2 % for the CuO-ZnO-CeO_2 catalyst. The presence of carbonates was also confirmed by the O 1s XPS band centered at high binding energy (531.9 eV and 531.4 eV, respectively for CuO-ZnO-CeO_2 (Fig. 7a) and CuO-ZnO-Al_2O_3 (Fig. 7b).

The XPS spectrum of Ce 3d for the CuO-ZnO-CeO_2 sample is depicted in Fig.8 and presents a complex behavior. The split of the band into numerous peak is due to the hybridization between the final state Ce 4f orbitals and the O 2p oxygen orbital [76]. In Fig.8 the peaks are identified by V and U labels, indicating respectively the spin orbit coupling 3 $d^{3/2}$ and $3d^{5/2}$ [77], by applying the convention introduced by Burroughs et al. [78] in 1976.

Ce3d spectrum can be decomposed in 5 doublets, (U''', V'''), (U'', V''), (U', V'), (U°, V°), and (U,V), corresponding to the emissions from the spin-orbit split $3d^{3/2}$ and $3d^{5/2}$ core levels [77-79]. The five doublets were assigned to different final states of tetravalent (Ce^{4+}) or trivalent (Ce^{3+}) in Ce compounds (see Table 3); U''' (916.6 eV) and V''' (898.2 eV) were due to a Ce $3d^9 4f^0$ $O2p^6$ final state, U'' (907.4 eV) and V'' (888.8 eV) to a Ce $3d^9 4f^1$ $O2p^5$ final state, U' (903.2 eV) and V' (884.9 eV) to a Ce $3d^9 4f^1$ $O2p^6$ final state, U° (899.3 eV) and V° (881.0 eV) to a Ce $3d^9 4f^2$ $O2p^5$ final state, and U (900.8 eV) and V (882.4 eV) to a Ce $3d^9 4f^2$ O $2p^4$ final state. Especially the well-defined U''' peak at 916.6 eV was characteristic of the presence of Ce^{4+} [77].

3.2. Catalytic tests

In order to verify the catalytic performances of the binary and ternary polyol catalysts in relation to the chemical composition, oxide structure and surface properties, CO_2 hydrogenation to methanol was used as test reaction. The tests were carried-out at atmospheric pressure by feeding the tubular reactor with a H_2/CO_2 =1/9 mixture. Methanol and methane were the main carbon containing products, while only traces of carbon monoxide were detected.

The activity of the four catalysts was compared at 240 °C (Fig.9). The binary catalysts, $CuO\text{-}CeO_2$ and $ZnO\text{-}CeO_2$, did not show any catalytic activity (CO_2 conversion below 2%). The ternary $CuO\text{-}ZnO\text{-}CeO_2$ and $Cu\text{-}ZnO\text{-}Al_2O_3$ catalysts showed similar conversion curves as a function of time, with stabilization of their activity after 4h reaction. The $CuO\text{-}ZnO\text{-}CeO_2$ catalyst showed the best result with a maximum conversion of about 20%, while $Cu\text{-}ZnO\text{-}Al_2O_3$ reached a conversion not exceeding 14%. The enhanced activity of the ternary catalysts is attributed to the synergistic effect between CuO and ZnO, as already known from the literature [80-82]. The higher activity of the $CuO\text{-}ZnO\text{-}CeO_2$ catalyst can be attributed to both the basicity of CeO_2 [83], which favors the adsorption of CO_2 (that is an acid molecule), and

the enhanced reducibility of the system, leading to the increase of the number of active sites after the reducing pretreatment operated in-situ, before the reaction tests. Moreover, in the Cu-ZnO-Al_2O_3 catalyst, copper and zinc oxides were not fully available due to the formation of the $CuAl_2O_4$ and $ZnAl_2O_4$ spinels, as shown by XRD. Indeed, zinc and copper trapped into the spinel cannot enter in intimate contact and their synergistic catalytic effect [81-83] cannot be deployed.

On the most active catalyst (CuO-ZnO-CeO_2), further tests, at different reaction temperature, were performed. The CO_2 conversion as a function of time is plotted in Fig.10a for the tests performed in the 190-240 °C temperature range. At the beginning the curves presented an activation step, characterized by a steep section of the conversion curve; after 1 h reaction, the change of slop indicated that the stationary state is going to be reached up (maximum CO_2 conversion). A slightly different behavior was observed for the test performed at 240 °C in which the approach to the maximum conversion was slower and characterized by a change in slope. By increasing the temperature, the selectivity to CH_4 increased, while the methanol selectivity decreased simultaneously (Fig. 10b). Methanol selectivity was favored at low temperature; MeOH is indeed unstable at high temperature and is transformed into CH_4 and H_2O (in presence of hydrogen) through the following successive reactions:

$$CO_2 + H_2 \longrightarrow CH_3OH + H_2 \longrightarrow CH_4 + H_2O$$

This transformation explains also the change in slope of the CO_2 conversion curve in Fig. 10a; at first the slope of the 240 °C curve followed that of the curves at lower temperature, while when the transformation to CH_4 started, the slope decreased and the rate for reaching the stationary state slowed-down.

4. Conclusions

The catalysts prepared by the polyol method, and reported in the present research, presented improved properties in terms of metal oxide dispersion, and morphology (i.e. sponge like shape for the CeO_2-containing catalysts), and a variety of the metal and metal oxide species on the surface. Moreover, the CuO-ZnO-CeO_2 and Cu-ZnO-Al_2O_3 catalysts exhibited a higher activity and selectivity in the methanol synthesis by CO_2 hydrogenation than those displayed by catalysts prepared by more conventional methods, as summarized in Table 3. The results obtained for the catalysts prepared in the present work are also reported for comparison.

Table 3: catalytic performances in the hydrogenation of CO_2, obtained on the catalysts prepared

Type of catalyst	Preparation method	T (°C)	P (MPa)	R (H_2/CO_2)	CO_2 conversion (%)	CH_3OH Selectivity (%)	Ref.
CuO-ZnO-Al2O_3	Polyol method	240	0.1	9.0	14	86	this
CuO-ZnO-CeO_2	Polyol method	240	0.1	9.0	20	90	work
CuO/ZnO/Al_2O_3	Solvent free routine	240	3.0	3.0	16	64	[40]
CuO/ZnO/ZrO_2	Surfactant co-precipitation method	240	3.0	3.0	12	33	[16]
CuO-ZnO-ZrO_2 (M)	Co-precipitation microfluidic	240	5.0	3.0	9	47	[41]
CuO-ZnO-ZrO_2 (pH)	Co-precipitation at controlled pH				14	50	
CZZ0	Precipitation/reduction method ($NaBH_4$)	230	5.0	3.0	17	67	[15]
CZZ3					15	62	
CZZ5					15	67	
Cu/ZnO	Co-precipitation	240	3.0	3.0	17	78	[84]
10Cu-/CeO_2	Coprecipitation + impregnation	230	3.0	3.0	4	66	[85]
0.5Pd-10Cu/CeO_2					6	49	
2Pd-10Cu/CeO_2					15	29	
CuO-ZnO-TiO_2-ZrO_2	Co-precipitation (oxalate)	240	3.0	3.0	17	44	[61]
Cu/ZnO	Impregnation	240	0.1	9.0	5	12	[42]
Cu-Zn/SiO_2	Impregnation	250	2.0	3.0	2	66	[1]
5%CuZn/rGo	Incipient wetness impregnation	250	1.5	3.0	14	3	[19]
10%CuZn/rGo					26	5	
20%CuZn/rGo					19	9	
CuO/ZnO/Al_2O_3 (Cp)	With Internal cooling water	240	3.0	3.0	52	69	[86]
CuO/ZnO/Al_2O_3 (Cp)	Without Internal cooling water						
Cu/ZrO_2+CaO	Wetness impregnation	250	0.1	3.0	3	1	[87]

The most part of the catalysts listed in Table 3 presented CO_2 conversion lower than 20 % and selectivity to methanol lower than 65%, even when the reaction was performed at relatively high pressure (1.5-5.0 MPa), a more favorable condition than that used in the present research. It is worth to notice that on catalysts prepared by impregnation [42], the reaction performed at atmospheric pressure, and with a H_2/CO_2 ratio of 9, allowed to obtain only 12% conversion and 70% selectivity to methanol at 240°C, confirming that polyol method is promising for the preparation of active catalysts for CO_2 hydrogenation (20% CO_2 conversion and 90% selectivity to MeOH).

Acknowledgements

All physico-chemical characterizations were performed by the technical platforms of IS2M. The authors are very grateful to S. Hajjar, L. Josien, L. Michelin, H. Nouali for their contribution.

References

[1] N.Yang, R. Wang, Sustainable technologies for the reclamation of greenhouse gas CO_2, J. Cleaner. Produc. 103 (2015) 784-792.

[2] I. Melian-Cabrera, M.L. Granados, J.L.G. Fierro, Pd-modified Cu–Zn catalysts for methanol synthesis from CO_2/H_2 mixtures: catalytic structures and performance, J. Catal. 210 (2002) 285-294.

[3] M. Matzen, Y. Demirel, Methanol and dimethyl ether from renewable hydrogen and carbon dioxide: Alternative fuels production and life-cycle assessment, J. Cleaner Produc. 139 (2016) 1068-1077.

[4] M.J. Bos, D.W.F. Brilman, A novel condensation reactor for efficient CO_2 to methanol conversion for storage of renewable electric energy, Chem. Eng. J. 278 (2015) 527-532.

[5] W. Wang, S. Wang, X. Ma, J. Gong, Recent advances in catalytic hydrogenation of carbon dioxide, Chem. Soc. Rev. 40 (2011) 3703-3727.

[6] T. Witoon, T. Permsirivanich, N. Kanjanasoontorn, C. Akkaraphataworn, A. Seubsai, K. Faungnawakij, C. Warakulwit, M. Chareonpanich, J. Limtrakul, Direct synthesis of dimethyl ether from CO_2 hydrogenation over Cu-ZnO-ZrO_2/SO_4^{2-} ZrO_2 hybrid catalyst: effects of sulfur-to-zirconia ratios, Catal. Sci.Technol. 5 (2015) 2347-2357.

[7] G. A. Olah, A. Goeppert, G. S. Prakash, Chemical recycling of carbon dioxide to methanol and dimethyl ether: from greenhouse gas to renewable, environmentally carbon neutral fuels and synthetic hydrocarbons, J. Org. Chem.74 (2008) 487-498.

[8] K.C. Waugh, Methanol synthesis, Catal.Lett.142 (2012)1153-1166.

[9] J.B. Hansen, P.E Højlund Nielsen, Methanol synthesis, Handbook of heterogeneous catalysis (2008).

[10] H. Arakawa**,** J.L. Dubois, K. Sayama, Selective conversion of CO_2 to methanol by catalytic hydrogenation over promoted copper catalyst, Energy. Convers. Mgmt. 1933 (1992) 521-528.

[11] M. Saito, T. Fujitani, I. Takahara, T. Watanabe, M. Takeuchi, Y. Kanai, K. Moriya, T. Kakumoto, Development of Cu/ZnO-based high performance catalysts for methanol synthesis by CO_2 hydrogenation, Energy. Convers. Mgmt. 36 (1995) 577-580.

[12] K-W. Jun, W-J. Shen, K-W. Lee, T. Inui, H. Hara, T. Takeguchi, J.B. Kim, Concurrent Production of Methanol and Dimethyl Ether from Carbon Dioxide Hydrogenation: Investigation of Reaction Conditions, Kor. Chem. Soc. 20 (1999) 993-998.

[13] K.Ushikoshi, K. Mori, T. Watanabe, M. Takeuchi, M. Saito, A 50 kg/day class test plant for methanol synthesis from CO_2 and H_2, Stud. Surf. Sci. Catal. 114 (1998) 357-362.

[14] T. Witoon, T. Permsirivanich., W. Donphai, A. Jaree, M. Chareonpanich. CO_2 hydrogenation to methanol over Cu/ZnO nano catalysts prepared via a chitosan-assisted co-precipitation method, Fuel. Process. Technol. 116 (2013) 72-78.

[15] X. Dong, F. Li, N. Zhao, F. Xiao, J. Wang, Y. Tan, CO_2 hydrogenation to methanol over Cu/ZnO/ZrO_2 catalysts prepared by precipitation-reduction, method. Appl. Catal., B. 191 (2016) 8-17.

[16] L. Li, D. MAO, J. YU, X. Guo, Highly selective hydrogenation of CO_2 to methanol over CuO-ZnO-ZrO_2 catalysts prepared by a surfactant-assisted co-precipitation method, J. Power. Sources. 279 (2015) 394-404.

[17] X. Guo, D. Mao, G. Lu, S. Wang, G. Wu, CO_2 hydrogenation to methanol over Cu/ZnO/ZrO_2 catalysts prepared via a route of solid-state reaction, Catal. Commun. 12 (2011) 1095-1098.

[18] A. Ateka, I. Sierra, J. Ereña, J. Bilbao, A.T. Aguayo, Performance of CuO-ZnO-ZrO_2 and CuO-ZnO-MnO as metallic functions and SAPO-18 as acid function of the catalyst for the synthesis of DME co-feeding CO_2, Fuel. Process. Technol, 152 (2016) 34-45.

[19] V. Deerattrakul, P. Dittanet, M. Sawangphruk, P. Kongkachuichay, CO_2 hydrogenation to methanol using Cu-Zn catalyst supported on reduced graphene oxide nanosheets, J. CO_2. Util. 16 (2016)104-113.

[20] L.X. Zhang, Y.C. Zhang, S.Y. Chen, Effect of promoter TiO_2 on the performance of $CuO-ZnO-Al_2O_3$ catalyst for CO_2 catalytic hydrogenation to methanol, J. Fuel Chem. and Tech. 39 (2011) 912-917.

[21] C. Huang, S. Chen, X. Fei, D. Liu, Y. Zhang, Catalytic hydrogenation of CO_2 to methanol: study of synergistic effect on adsorption properties of CO_2 and H_2 in $CuO/ZnO/ZrO_2$ system, J. Catalysts, 5(2015) 1846-1861.

[22] B.J. Liaw and Y.Z. Chen, Liquid-phase synthesis of methanol from CO_2/H_2 over ultrafine CuB catalysts, J. App. Catal. A. 206 (2001) 245-256.

[23] P.S.S. Prasad, J.W. Bae, K.W. Jun, K.W. Lee, Fischer–Tropsch Synthesis by Carbon Dioxide Hydrogenationon Fe-Based Catalysts, J. Cat. Surv. Asia. 12(2008)170-183.

[24] T. Inoue, T. Iizuka, K. Tanabe, Support Effect of Zinc Oxide Catalyst on Synthesis of Methanol from CO_2 and H_2, Bull. Chem. Soc. Jpn. 60 (1987) 2663-2664.

[25] I. Melian-Cabrera, M. Lopez Granados, P. Terreros, J. L. G. Fierro, CO_2 hydrogenation over Pd-modified methanol synthesis catalysts, Catal. Today. 45 (1998) 251-256.

[26] B. Denise, R. P. A. Sneeden, Oxide-supported copper catalysts prepared from copper formate: Differences in behavior in methanol synthesis from CO/H_2 and CO_2/H_2 mixtures, Appl. Catal. 28 (1985) 235-239.

[27] E. Ramaroson, R. Kieffer, A. Kiennemenn, Reaction of $CO-H_2$ and CO_2-H_2 on copper-zinc catalysts promoted by metal oxides of groups III and IV, Appl. Catal. 4 (1982) 281-286.

[28] F. Arena, K. Barbera, G. Italiano, G. Bonura, L. Spadaro, F. Frusteri, Synthesis, characterization and activity pattern of $Cu-ZnO/ZrO_2$ catalysts in the hydrogenation of carbon dioxide to methanol, J. Catal. 249 (2007) 185-194.

[29] X.M. Liu, G.Q. Lu, Z.F. Yan, J. Beltramini, Recent Advances in Catalysts for Methanol Synthesis via Hydrogenation of CO and CO_2, Ind. Eng. Chem. Res. 42 (2003) 6518-6530.

[30] Z.S. Hong, Y. Cao, J.F. Deng, K.N. Fan, CO_2 Hydrogenation to Methanol Over $Cu/ZnO/Al_2O_3$ Catalysts Prepared by a Novel Gel-Network-Co-precipitation Method, Catal. Lett. 82 (2002) 37-44.

[31] C.L. Chiang, K.S. Lin, H.W. Chuang, Direct synthesis of formic acid via CO_2 hydrogenation over $Cu/ZnO/Al_2O_3$ catalyst, J. Cleaner. Produc. 172 (2018) 1957-1977.

[32] Y. Nitta, T. Fujimatsu, Y. Okamoto, T. Imanaka, Effect of starting salt on catalytic behaviour of $Cu-ZrO_2$ catalysts in methanol synthesis from carbon dioxide, Catal. Lett. 17 (1993) 157-165.

[33] J. Słoczynski, R. Grabowski, A. Kozłowska, P. Olszewski, J. Stoch, J. Skrzypek, M. Lachowska, Catalytic activity of the $M/(3ZnO\cdot ZrO_2)$ system (M = Cu, Ag, Au) in the hydrogenation of CO_2 to methanol, Appl. Catal. A: Gen. 278 (2004) 11-23.

[34] J. Słoczynski, R. Grabowski, A. Kozłowska, P. Olszewski, M. Lachowska, J. Skrzypek, J. Stoch, Effect of Mg and Mn oxide additions on structural and adsorptive properties of $Cu/ZnO/ZrO_2$ catalysts for the methanol synthesis from CO_2, Appl. Catal. A: Gen. 249 (2003) 129-138.

[35] R. Raudaskoski, M.V. Niemelä, R.L. Keiski, The effect of ageing time on co-precipitated $Cu/ZnO/ZrO_2$ catalysts used in methanol synthesis from CO_2 and H_2, Top. Catal. 45 (2007) 57-60.

[36] Y. Choi, K. Futagami, T. Fujitani, J. Nakamura,The role of ZnO in Cu/ZnO methanol synthesis catalysts-morphology effect or active site model, Appl. Catal. A: Gen. 208 (2001)163-167.

[37] G. X. Qi, J. H. Fei, X. M. Zheng, Z. Y. Hou, Effect of Titanium on Methanol Synthesis from CO_2 Hydrogenation over $Cu/\gamma\text{-}Al2O_3$, Chin. Chem. Lett. 12 (2001) 537-540.

[38] R.A. Köppel, C. Stöcker, A. Baiker, Copper-and silver–zirconia aerogels: preparation, structural properties and catalytic behavior in methanol synthesis from carbon dioxide, J. Catal. 179 (1998) 515-527.

[39] C.L. Carnes, K.J. Klabunde, The catalytic methanol synthesis over nanoparticle metal oxide catalysts, J. Mol. Catal. A: Chem. 194 (2003) 227-236.

[40] H. Lei, Z. Hou, J. Xie, Hydrogenation of CO_2 to CH_3OH over $CuO/ZnO/Al_2O_3$ catalysts prepared via a solvent-free routine, Fuel 164 (2016)191-198.

[41] L. Angelo, M. Girleanu, O. Ersen, C. Serra, K. Parkhomenko, A.C. Roger. Catalyst synthesis by continuous co-precipitation under micro-fluidic conditions: Application to the preparation of catalysts for methanol synthesis from CO_2/H_2. Catal. Today, 270 (2016) 59-67.

[42] J. Díez-Ramírez, F. Dorado, A.R. de la Osa, J.L. Valverde, P. Sánchez, Hydrogenation of CO_2 to methanol at atmospheric pressure over Cu/ZnO catalysts: influence of the calcination, reduction, and metal loading, Ind. Eng. Chem. Res. 56 (2017) 1979-1987.

[43] M. Lortie, R. Isaifan, Y. Liu, S. Mommers, Synthesis of CuNi/C and $CuNi/Al_2O_3$ Catalysts for the Reverse Water Gas Shift Reaction, Int. J. Chem. Eng. (2015)

[44] Y. Jeong, J. Y. Kang, I. Kim, H. Jeong, J. K. Park, J. H. Park, J. C. Jung, Preparation of Cu/ZnO catalyst using a polyol method for alcohol-assisted low temperature methanol synthesis from syngas, Korean. J. Chem. Eng. 33 (2016) 114-119.

[45] H. S. Wu, S. C. Chung, Kinetics of hydrogen production of methanol reformation using $Cu/ZnO/Al_2O_3$ catalyst, J. Comb. Chem. 9 (2007) 990-997.

[46] B.K. Park, S. Jeong, D. Kim, J. Moon, S. Lim, J.S. Kim, Synthesis and size control of monodisperse copper nanoparticles by polyol method, J. Colloid. Interface. Sci. 311 (2007) 417-424.

[47] T.G. Altinçekiç, I. Boz, Influence of synthesis conditions on particle morphology of nanosized Cu/ZnO powder by polyol method, Bull. Mater. Sci. 31 (2008) 619-624.

[48] L. F. Bobadilla, C. Garcia, J.J. Delgado, O. Sanz, F. Romero-Sarria, M.A. Centeno, J.A. Odriozola, Influence of PVP in magnetic properties of NiSn nanoparticles prepared by polyol method, J. Magn. Magn. Mater. 324 (2012) 4011-4018.

[49] C. Y. Lu, H. H. Tseng, M. Y. Wey, L. Y. Liu, K.H. Chuang. Effects of the ratio of Cu/Co and metal precursors on the catalytic activity over Cu-Co/Al_2O_3 prepared using the polyol process, MATER. SCI. ENG. B. 157 (2009) 105-112.

[50] K. H. Chuang, K. Shih, C.Y. Lu, M.Y. Wey, Copper catalysts prepared via microwave-heated polyol process for preferential oxidation of CO in H_2-rich streams, Int. J. Hydrog. Energy. 38 (2013) 100-108

[51] K.C Song, S.M. Lee, T.S. Park, B.S. Lee, Preparation of colloidal silver nanoparticles by chemical reduction method, Korean J. Chem. Eng.26 (2009) 153-155.

[52] J.H. Byeon, Y.W. Kim, A novel polyol method to synthesize colloidal silver nanoparticles by ultrasonic irradiation, Ultrason. Sonochem 19 (2012) 209-215.

[53] Y. Jeong, J.Y. Kang, I. Kim, H. Jeong, J.K. Park, J.H. Park, J. C. Jung, Preparation of Cu/ZnO catalyst using a polyol method for alcohol-assisted low temperature methanol synthesis from syngas, Korean. J. Chem. Eng., 33 (2016) 114-119.

[54] İ. Boz, T.G. Altınçekiç Liquid phase hydroxylation of benzene to phenol over Cu/ZnO catalysts, React. Kinet. Mech.cat. 102 (2011) 195-205.

[55] E. Bayrakdar, T.G. Altınçekiç, M.A.F. Öksüzömer, Effects of PVP on the preparation of nanosized Al_2O_3 supported Ni catalysts by polyol method for catalytic partial oxidation of methane, Fuel. Process. Technol.110 (2013) 167-175.

[56] S. Brunauer, S. P. H. Emmett, E. Teller, Absorption of gases in multi molecular layers, J. Am. Chem. Soc. 60 (1938) 309-319.

[57] E.P. Barrett, L.G. Joyner, P.P. Halenda, The determination of pore volume and area distributions in porous substances. I. Computations from nitrogen isotherms, J. Am. Chem. Soc. 73 (1951) 373-380.

[58] S.B. Bagherzadeh, M. Haghighi, and N. Rahemi, Novel oxalate gel co-precipitation synthesis of ZrO_2-CeO_2-promoted CuO-ZnO-Al_2O_3 nanocatalyst for fuel cell-grade hydrogen production from methanol: Influence of ceria-zirconia loading, Energy. Convers. Manage. 134(2017)88-102.

[59] B. Ouyang, W. Tan, B. Liu, Morphology effect of nanostructure ceria on the Cu/CeO_2 catalysts for synthesis of methanol from CO_2 hydrogenation, Catal. Commun. 95(2017) 36-39.

[60] H. Ajamein, M. Haghighi, On the microwave enhanced combustion synthesis of CuO–ZnO–Al_2O_3nanocatalyst used in methanol steam reforming for fuel cell grade hydrogen production: effect of microwave irradiation and fuel ratio, Energy. Convers. Manage.118 (2016) 231-242.

[61] J. Xiao, D. Mao, X. Guo, J. Yu, Effect of TiO_2, ZrO_2, and TiO_2-ZrO_2 on the performance of CuO-ZnO catalyst for CO_2 hydrogenation to methanol, Appl. Surf. Sci. 338 (2015) 146-153.

[62] T. Witoon, N. Kachaban, W. Donphai, P. Kidkhunthod, K. Faungnawakij, M. Chareonpanich, J. Limtrakul. Tuning of catalytic CO_2 hydrogenation by changing composition of CuO-ZnO-ZrO_2 catalysts, Energy. Convers. Manage. 118 (2016) 21-31.

[63] J. Aguado, M.C. Castro, Influence of the thermal treatment upon the textural properties of sol-gel mesoporous γ-alumina synthesized with cationic surfactants, Micropor. Mesopor. Mat. 128 (2010) 48-55.

[64] V. Deerattrakul, P. Dittanet, M. Sawangphruk, P. Kongkachuichay, CO_2 hydrogenation to methanol using Cu-Zn catalyst supported on reduced graphene oxide nanosheets, J. CO_2 UTIL. 16 (2016) 104-113

[65] F. Prinetto, G. Ghiotti, P. Graffin, D. Tichit, Synthesis and characterization of sol–gel Mg/Al and Ni/Al layered double hydroxides and comparison with co-precipitated samples, Micropor. Mesopor. Mat. 39 (2000) 229-247.

[66] Y. Zhu, X. Kong, D.B. Cao, J. Cui, Y. Zhu, Y.W. Li.The rise of calcination temperature enhances the performance of Cu catalysts: contributions of support, ACS. Catal. 4 (2014) 3675-3681.

[67] J. Liu, C. H. Han, X. Yang, G. Gao, Q. Shi, M. Tong, C. Li, Methyl formate synthesis from methanol on titania supported copper catalyst under UV irradiation at ambient condition: Performance and mechanism, J. Catal. 33 (2016) 162-170

[68] X. Dong, F. Li, N. Zhao, Y. Tan, J. Wang, F. Xiao, CO_2 hydrogenation to methanol over Cu/Zn/Al/Zr catalysts prepared by liquid reduction, Chinese. J. Catal. 38 (2017) 717-725.

[69] B. Zhang, Y. L. Zhu, G. Q. Ding, H. Y. Zheng, Y. W. Li, Modification of the supported Cu/SiO2 catalyst by alkaline earth metals in the selective conversion of 1, 4-butanediol to γ-butyrolactone, Appl. Catal. A. 443 (2012) 191−201.

[70] S. Murcia-Mascarós, R. M. Navarro, L. Gomez-Sainero. Oxidative methanol reforming reactions on CuZnAl catalysts derived from hydrotalcite-like precursors, J. Catal. 198 (2001) 338-347.

[71] K. Sun, K.W. Lu, F. Qiu, S. Liu, X. Xu, Direct synthesis of DME over bifunctional catalyst: surface properties and catalytic performance, Appl. Catal. A. 252 (2003) 243-249.

[72] R.M. Friedman, J.J. Freeman, F.W. Lytle, Characterization of $CuAl_2O_3$ catalysts, J. Catal, 55 (1978) 10-28.

[73] M. C. Biesinger, L.W. Lau, A.R. Gerson, R.S.C. Smart, Resolving surface chemical states in XPS analysis of first row transition metals, oxides and hydroxides: Sc, Ti, V, Cu and Zn, Appl. Surf. Sci. 257 (2010) 887-898.

[74] Y. K. Gao, F. Traeger, O. Shekhah, H. Idriss, C. Wöll, Probing the interaction of the amino acid alanine with the surface of ZnO (101), J. Colloid. Interface. Sci. 338 (2009) 16-21.

[75] C. Yang, F. Bebensee, J. Chen, X. Yu, A. Nefedov, C. Woll, Carbon dioxide adsorption on CeO_2(110): an XPS and NEXAFS study, Chem. Phys. Chem. 18 (2017) 1874-1880

[76] L. Óvári, S. K. Calderon, Y. Lykhach, J. Libuda, A. Erdőhelyi, C. Papp, H. P. Steinrück, Near ambient pressure XPS investigation of the interaction of ethanol with Co/CeO_2 (1 1 1), J. Cat. 307 (2013) 132-139.

[77] A. Pfau, K.D. Schierbaum, The electronic structure of stoichiometric and reduced CeO_2 surfaces: an XPS, UPS and HREELS study, Surf. Sci. 321 (1994) 71-81.

[78] P. Burroughs, A. Hamnett, A.F. Orchard, G. Thorton, Satellite structure in the X-ray photoelectron spectra of some binary and mixed oxides of lanthanum and cerium, J. Chem. Soc. Dalton Trans. 17 (1976) 1686-1698.

[79] C.J. Nelin, P.S. Bagus, E.S. Ilton, S.A. Chambers, H. Kuhlenbeck, H.J. Freund, Relationships between complex core level spectra and materials properties, Int. J. Quantum. Chem. 110 (2010) 2752-2764.

[80] J. C. Frost, Junction effect interactions in methanol synthesis catalysts, Nature. 334 (1988) 577□ 580.

[81] R. Burch, R. J. Chappell, S. E. Golunski, Synergy between copper and zinc oxide during methanol synthesis. Transfer of activating species, J. Chem. Soc. Faraday Trans. 1 Phys. Chem. Condens. Phases. 85(1989) 3569□ 3578.

[82] R. Burch, R. J. Chappell, S. E. Golunski, Synergy at a distance in the synthesis of methanol over copper catalysts, Catal. Lett. 12 (1988) 439□ 443.

[83] X. Li, Z.J. Zhao, L. Zeng, J. Zhao, H. Tian, S. Chen, K. Li, S. Sang, J. Gong, On the role of Ce in CO_2 adsorption and activation over lanthanum species, Chem. Sci. 9 (2018) 3426-3437.

[84] H. Lei, R. Nie, G. Wu, Z. Hou, Hydrogenation of CO_2 to CH_3OH over Cu/ZnO catalysts with different ZnO morphology, Fuel, 154 (2015) 161-166.

[85] E.J. Choi, Y. H. Lee, D.W. Lee, D. J. Moon, K.Y. Lee, Hydrogenation of CO_2 to methanol over Pd-Cu/CeO_2 catalysts, Mol. Catal. 434 (2017) 146-153.

[86] W. Wu, K. Xie, D. Sun, X. Li, F. Fang, $CuO/ZnO/Al_2O_3$ Catalyst Prepared by Mechanical-Force-Driven Solid-State Ion Exchange and Its Excellent Catalytic Activity under Internal Cooling Condition, Ind. Eng. Chem. Res. 56 (2017) 8216-8223.

[87] S. Soisuwan, W. Wisaijorn, C. Nimnul, O. Maunghimpan, P. Praserthdam, The Combination of Calcium Oxide and Cu/ZrO_2 Catalyst and their Selective Products for CO_2 Hydrogenation, Eng. J. 20 (2016) 39-48.

No interest conflicts affect the authors of this manuscript.

FIGURES

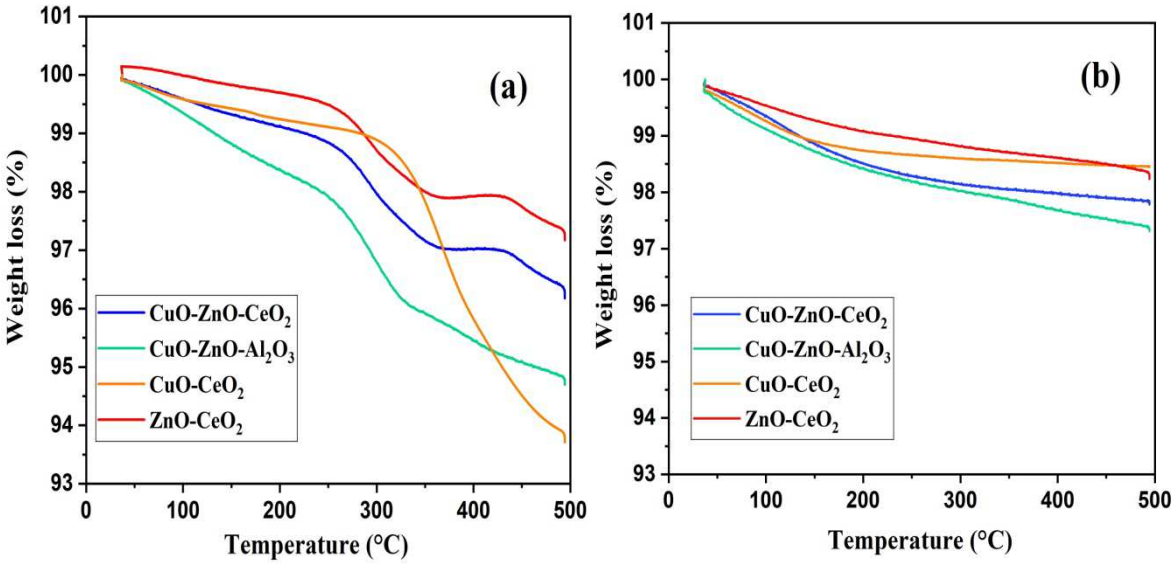

Fig.1. *TGA profiles of catalyst: (a) before calcination, (b) after calcination at 500 °C*

Courbes ATG des catalyseurs : a) avant calcination b) après calcination à 500 °C

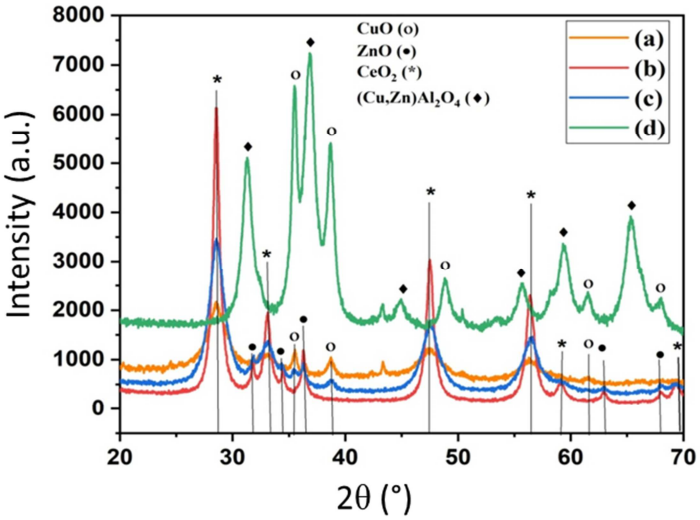

Fig.2. *XRD patterns of calcined catalysts: (a) CuO-CeO_2, (b) ZnO-CeO_2, (c) CuO-ZnO-CeO_2, and (d) CuO-ZnO-Al_2O_3.*

DRX des catalyseurs calcinés/ *(a) CuO-CeO_2, (b) ZnO-CeO_2, (c) CuO-ZnO-CeO_2, et (d) CuO-ZnO-Al_2O_3.*

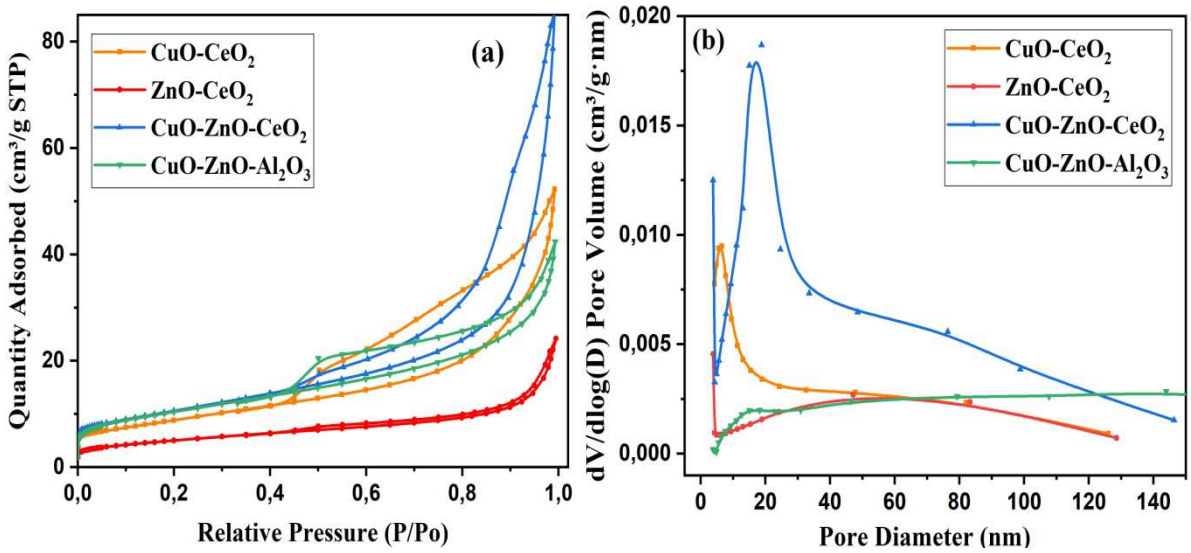

Fig.3. *(a) N_2-adsorption–desorption isotherms and (b) Pore size distribution, of all samples*

(a) Isothermes d'adsorption et désorption d'azote et (b) distribution poreuse des échantillons

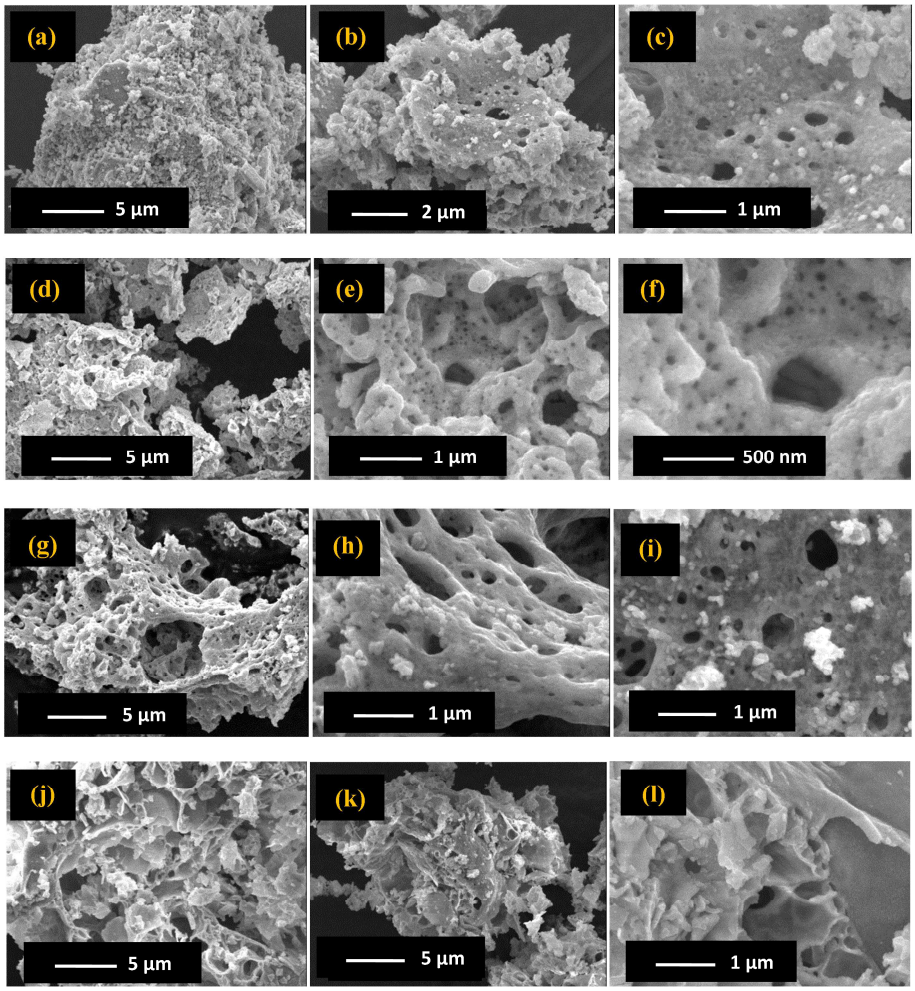

Fig.4. *SEM images at different magnification of all catalysts (a-c) CuO-CeO_2, (d-f) ZnO-CeO_2 (g-i) CuO-ZnO-CeO_2 and (j-l) CuO-ZnO-Al_2O_3*

Images MEB des catalyseurs (a-c) CuO-CeO_2, (d-f) ZnO-CeO_2 (g-i) CuO-ZnO-CeO_2 et (j-l) CuO-ZnO-Al_2O_3

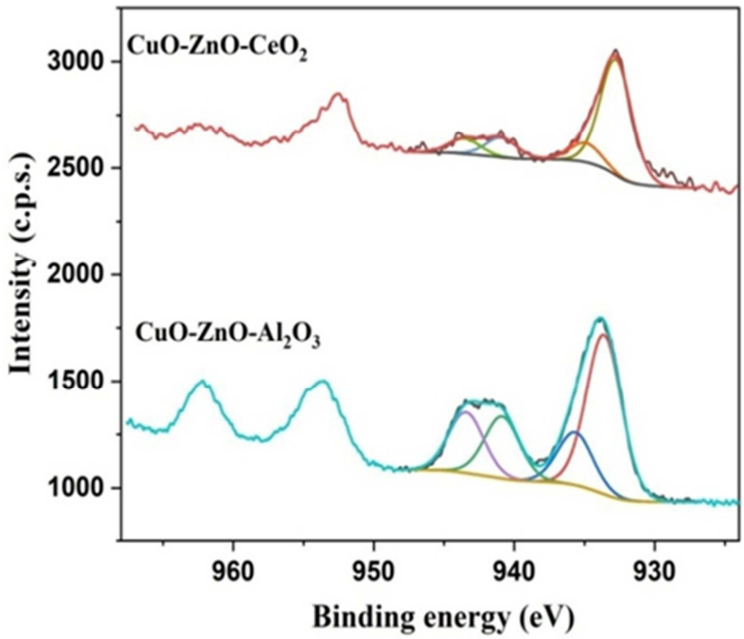

Fig.5. *Cu 2p XPS spectra of CuO-ZnO-CeO_2 and CuO-ZnO-Al_2O_3 samples*

Spectres XPS Cu 2p des échantillons CuO-ZnO-CeO_2 et CuO-ZnO-Al_2O_3

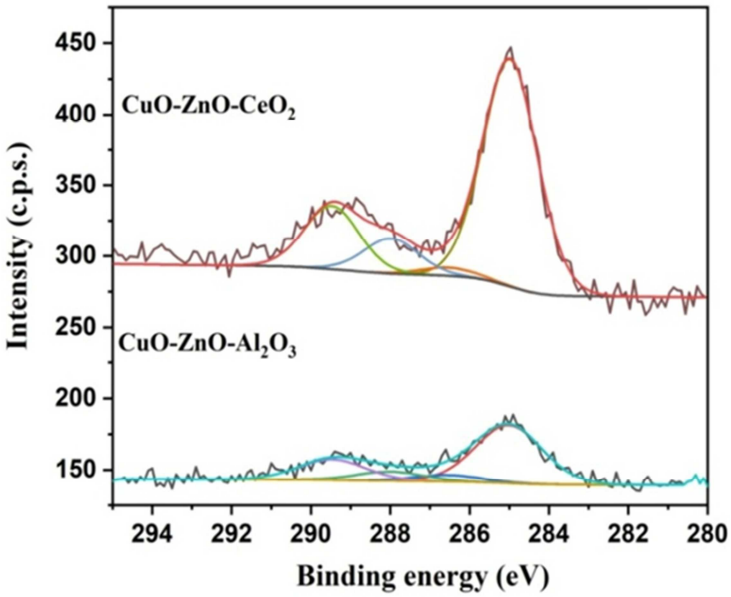

Fig.6. *C 1s XPS spectra of CuO-ZnO-CeO_2 and CuO-ZnO-Al_2O_3 samples*

Spectres XPS C 1s des échantillons CuO-ZnO-CeO_2 et CuO-ZnO-Al_2O_3

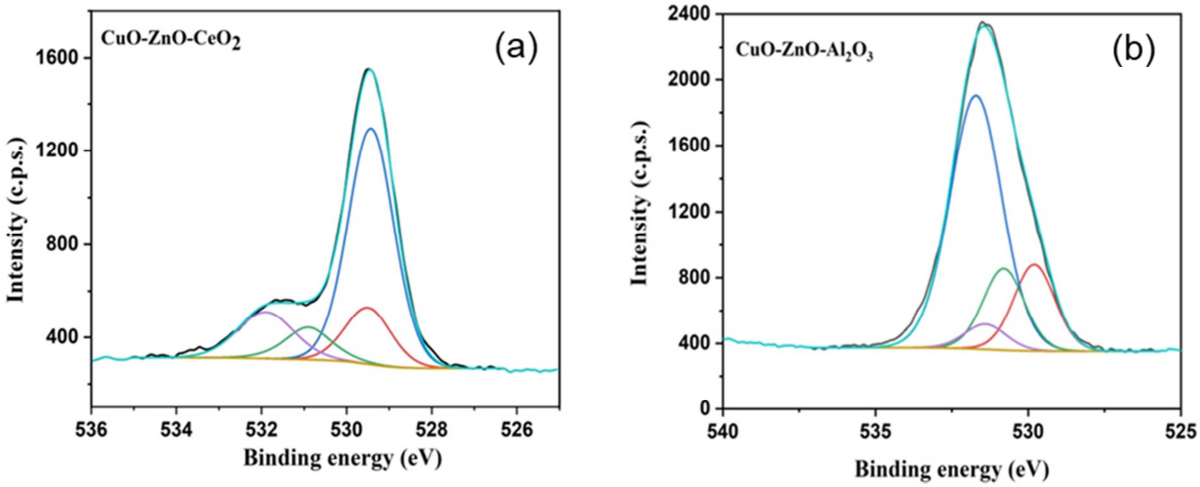

Fig.7. *O 1s XPS spectra of (a) CuO-ZnO-CeO_2 and (b) CuO-ZnO-Al_2O_3 samples*

Spectres XPS O 1s des échantillons (a) CuO-ZnO-CeO_2 et (b) CuO-ZnO-Al_2O_3

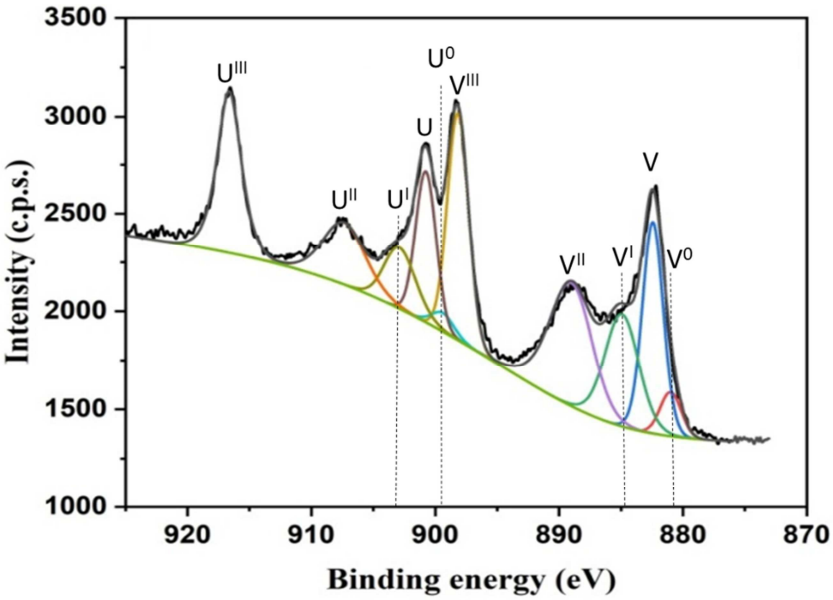

Fig.8. *Ce 3d XPS spectra of the CuO-ZnO-CeO_2 sample*

Spectres XPS Ce 3d de l'échantillon CuO-ZnO-CeO_2

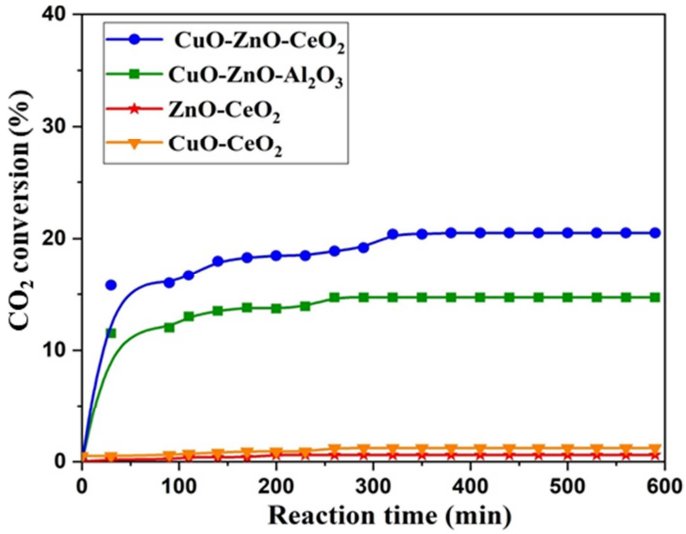

Fig.9. *CO_2 conversion as function of the time of reaction. Reaction conditions: CO_2/H_2 = 1/9, T=240°C, flow=1L.h^{-1} and P = 1 atm.*

Conversion de CO_2 en fonction du temps de réaction. Conditions de réaction : CO_2/H_2 = 1/9, T=240°C, débit=1L.h^{-1} et P = 1 atm.

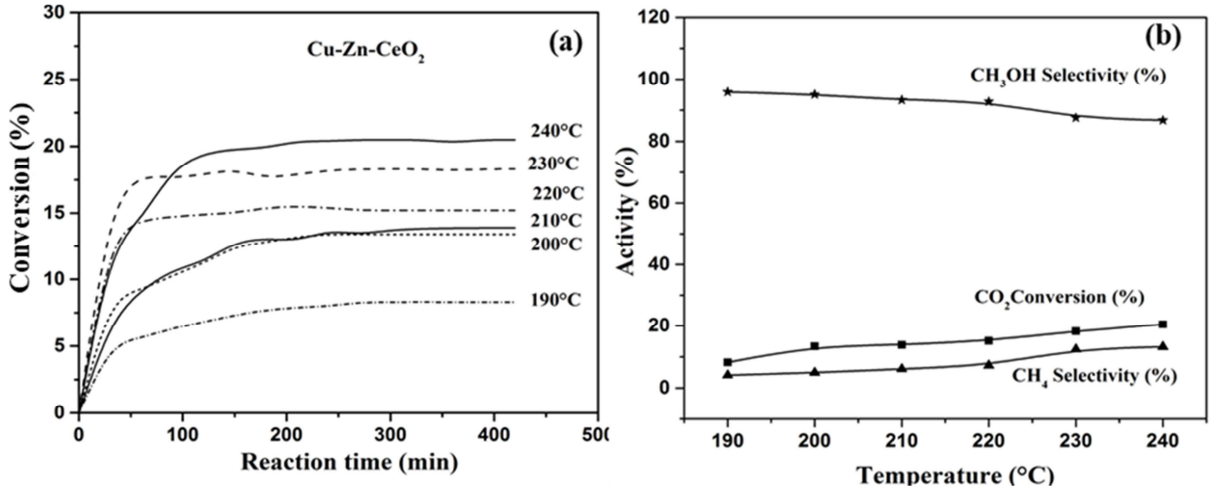

Fig.10. *a) CO_2 conversion as function of the time and temperature of reaction b)-MeOH and CH_4 selectivity as function of the temperature of reaction, over the CuO-ZnO-CeO_2 catalyst: flow=1L.h^{-1} and P = 1 atm*

a) Conversion de CO_2 en fonction du temps et de la température de réaction b) Sélectivités envers méthanol et méthane en fonction de la température de réaction pour le catalyseur CuO-ZnO-CeO_2 : débit=1L.h^{-1} et P = 1 atm